Undoing wavefield interference for AVAZ measurements

David C. Henley and Faranak Mahmoudian

ABSTRACT

There is a lot of interest in measuring the amplitudes of reflections from anisotropic rock layers in the earth. Such measurements can be used to estimate the rock layer's anisotropic elastic parameters. In the case of fracture-induced anisotropy, fracture orientation and intensity can be determined from these parameters. Most methods for estimating anisotropic elastic parameters require a set of reflection amplitude measurements as a function of both source-receiver offset and survey azimuth (AVAZ). A large problem with many of these measurements, however, is the interference between the targeted reflection event and other, shallower seismic events, or 'noise'. This interference can result in large amplitude disturbances of the target event, making accurate amplitude measurements impossible.

We show here how to remove most of this interference using radial trace (RT) filtering techniques. The RT filter method is attractive because it estimates and subtracts coherent components along various dip directions directly observed on the input trace gathers. Careful parameter selection ensures that amplitudes in the frequency band of the target reflection are unaffected by the noise subtraction. The resulting amplitude trend on each trace gather is much smoother, and a better fit to the theoretical trend. We demonstrate on a set of AVAZ survey data acquired at the CREWES physical modeling facility. Elastic parameters estimated from these measurements were verified elsewhere by an independent technique.

INTRODUCTION

Various advances in exploration technology, in both theory and seismic acquisition technology, have allowed the extraction of increasingly detailed information about subsurface rock layers and their elastic parameters for use in developing and producing hydrocarbon resources. The earliest use of seismic data was aimed only at determining the shape and configuration of subsurface 'structures' in order to estimate their potential as hydrocarbon reservoirs. As digital recording and processing were introduced, however, it became possible to use the relative amplitudes of reflections as additional information in the interpretation process. The effect of fluid content on reservoir rocks—the so-called 'bright spot' phenomenon—became an important tool for delineating the areal extent, and often the total reservoir volume, for a hydrocarbon prospect. Further developments in seismic theory led to the measurement of reflection amplitude as a function of 'offset' (actually reflection angle) for use as a sensitive detector of elastic parameter changes at rock layer boundaries. This AVO technology has been applied extensively to help delineate not only lateral changes in lithology along a rock layer, but changes in pore fluid content, as well.

More recently, theoretical and laboratory work have both indicated that the stiffness parameters of rock materials can be related not only to micro-layering and geometry of pore space, but also to systems of fractures of all sizes. Since fractures are important not

only as pore space, but also as fluid conduits, knowing their intensity and orientation is of great importance to engineers planning the drilling and development of a hydrocarbon field. Hence, it has become an important goal to accurately measure the anisotropy parameters of potential reservoir layers using seismic data. Since we generally do not know the orientation of fracture planes prior to a survey, data must be acquired at various offsets along several profiles over at least a 90 degree aperture of azimuth (AVAZ) in order to determine both the direction and 'strength' of the anisotropy in a layer, and hence the fracture orientation and intensity. While both shear and compressional wave components of the elastic wavefield can be measured and used for elastic parameter estimation, we use here only the compressional wave as measured by vertical component transducers in the physical modeling laboratory.

The theoretical and laboratory measurement details for this work are extensively covered elsewhere (Mahmoudian et al, 2013a); we demonstrate here only the processing for removing interference and exclude the application of various reflection amplitude compensation factors discussed by Mahmoudian et al (2012a, 2012b) and Wong and Mahmoudian (2011).

The physical model

The physical model featured in this study was constructed specifically for the purpose of measuring the seismic response of a layer with orthorhombic symmetry. The target layer was constructed of sheets of linen fabric bonded together with phenolic resin. Using traveltime analysis on this constructed phenolic layer, we found that the layer, although orthorhombic, approximates a layer with HTI symmetry (Mahmoudian et al, 2013c). Layers of isotropic Plexiglas were cemented to the upper and lower surfaces of the target layer, and the whole model immersed in water for the measurements. The water layer ensured that only compressional waves were transmitted and measured. Also, water does not support the large-amplitude surface waves that can dominate model data. The phenolic layer was subjected to a series of independent experiments prior to being incorporated into the larger model, and the processing of some of those measurements is described in more detail in Henley and Wong (2013). Figure 1 shows the model configuration, and the experimental procedure and setup are described in more detail in Mahmoudian et al (2012b).

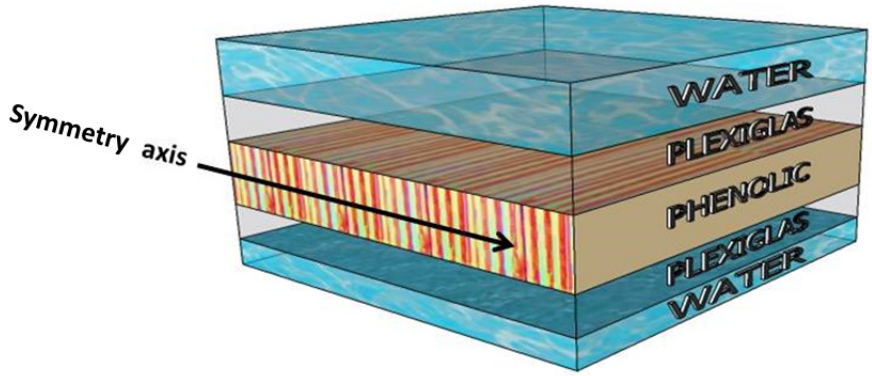

FIG. 1. The physical model over which the AVAZ reflection survey was performed. All azimuth angles for the survey are measured relative to the phenolic symmetry axis shown here.

The problem

In spite of the fact that a physical model provides the cleanest and most controlled environment for measuring and verifying elastic parameters, we can see in the shot gather acquired along the zero azimuth with respect to the phenolic symmetry axis, in Figure 2, that measuring the amplitude of the reflection from the top of the phenolic layer is not straightforward. Besides the water surface, there are only four reflecting interfaces in the model, and the upper two can be readily identified in Figure 2. On the other hand, because the source and receiver were deployed in water (the top-most layer), we see ghost events, associated with shot and receiver depth, present on each event in Figure 2—the direct arrivals as well as the two reflecting interfaces. These ghosts have the effect of making the effective event wavelets very long, leading to overlap and interference of the events. Aggravating the interference is the fact that the moveout velocity of the shallower reflection from the upper surface of the Plexiglas is much lower than that of the deeper reflection from the Plexiglas/phenolic boundary. The lower part of figure 3 shows the target reflection after NMO correction, with all the interfering events distorting its amplitude, while the upper portion shows a plot of reflection amplitudes, picked along the peak of the shallowest positive loop of the reflection at about 1315ms. The interference makes the amplitudes of this event essentially unmeasurable.

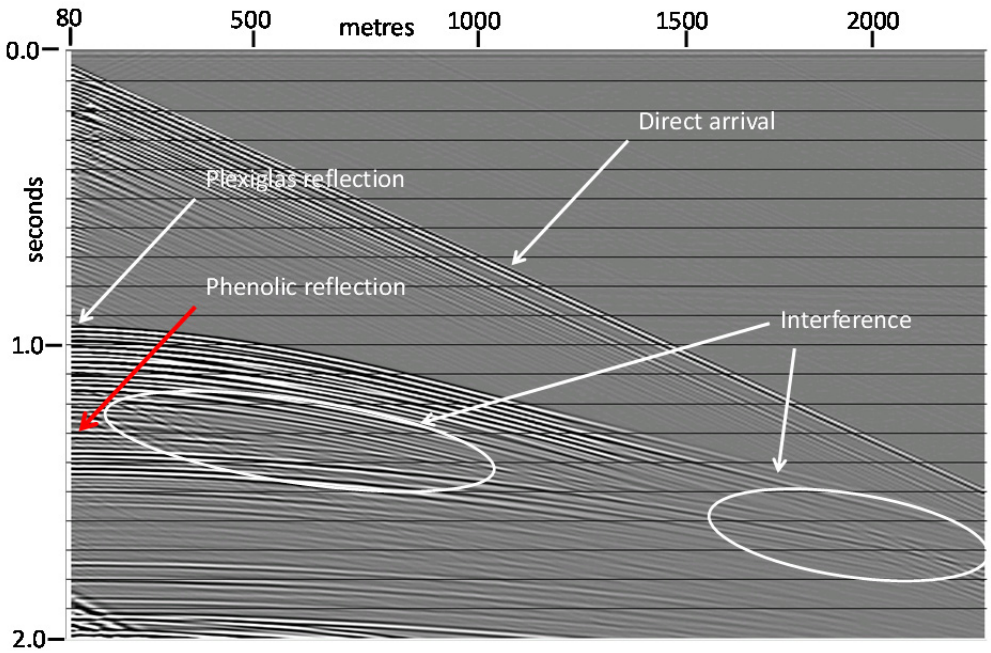

FIG. 2. The raw trace gather recorded over the physical model in Figure 1 at an azimuth of 0 degrees relative to the phenolic symmetry axis. The direct water arrival and the 'shallow' reflection from the top of the Plexiglas in the model both interfere significantly with the desired reflection from the top of the HTI layer.

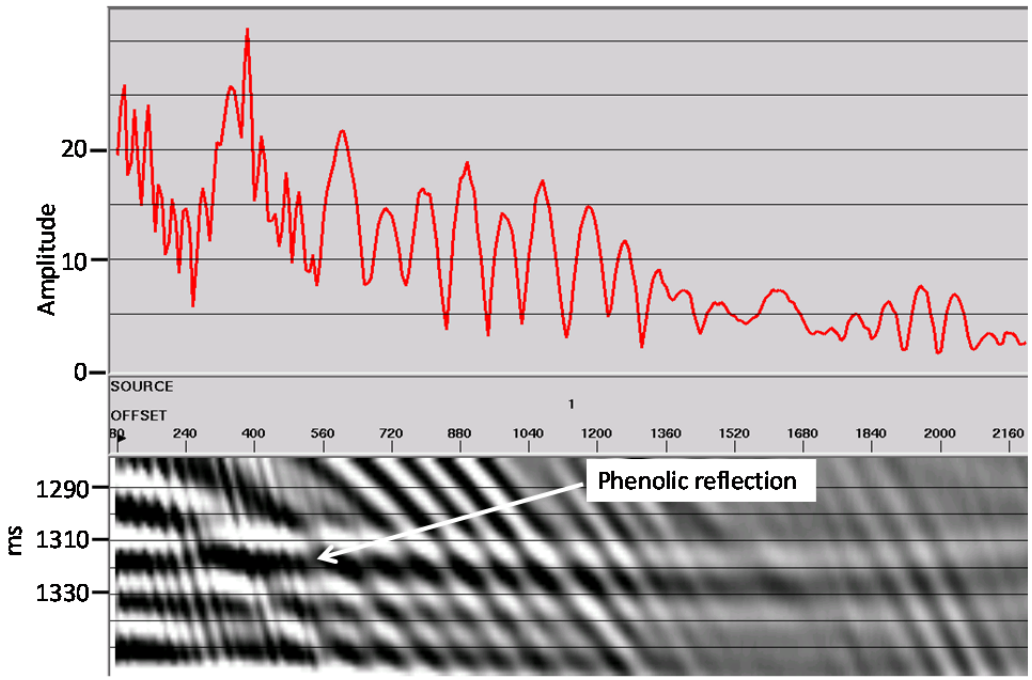

FIG. 3. Zoom of the interference on the phenolic reflection, and the effect of that interference on amplitude measurement.

METHOD

Since we are interested in preserving the amplitudes of the target reflection, we must choose a process for removal of the interference that does not alter those amplitudes. We chose to use our ProMAX radial trace (RT) filter module (Henley 2003, 2011), which allows us to design 'fan' filters aimed at attenuating all linear noise originating from a source point, as well as 'dip' filters aimed at attenuating all linear noise of a particular slope. The mechanism behind radial trace filtering is the fact that linear noises whose wavefronts align with radial trace trajectories in the original X-T domain have their apparent spectra shifted to much lower frequencies in the RT domain, often well-separated from the spectra of events, like reflections, that are *not* aligned with the trajectories. In the RT domain we apply a low-pass filter designed to exclude seismic reflection frequencies but to admit the low-apparent-frequency linear noise. The inverted RT transform then yields a good estimate of the coherent noise. Subtracting the noise estimate from the original trace gather removes the noise interference without affecting legitimate reflection amplitudes, since there is, due to careful parameter selection, no overlap in frequency between the noise estimate and the reflections.

This technique is very effective for linear noise whose apparent moveout is significantly different from that of underlying reflections. As the local slope of the noise wavefront approaches that of the reflections, however, the frequency separation effected by the radial trace transform becomes less complete, so that for linear noises nearly parallel to reflection wavefronts, the noise bandwidth in the RT domain begins to overlap the reflection bandwidth. This limitation arises in any wavefield separation method which relies on differential moveout, but seems less problematic for RT filtering than for other common methods like f-k filtering.

The actual procedure we used for removing interfering events from the phenolic layer reflection consisted of two stages. In the first stage, we applied a radial trace fan filter to the uncorrected source gather to attenuate all source-generated noises which are linear with source-receiver offset, as well as a radial trace dip filter to attenuate the ghost and repeated arrivals parallel to the direct arrival energy seen in Figure 2 For both these filter steps, care was taken to separate the frequencies passed by the filter from those of the underlying reflections. The second step of our procedure corrected the gather for NMO, using the estimated RMS velocity of the target reflection at 1315ms. This step flattened the phenolic event, except for the offset-related variation caused by departure from hyperbolic moveout. Flattening the event essentially increases the frequency separation between the reflection event and linear noises (in the RT domain), although the NMO correction itself introduces some lowering of reflection frequency due to waveform stretch at longer offsets. Using a zoomed display centred on this event, various pseudo-linear interfering events were analyzed and removed, one by one, using RT dip filters, until the target event was as clean as possible. For the actual amplitude measurements, described by Mahmoudian et al (2013a, 2013b, 2013c), NMO was restored to the data before measurement; but for the displays shown in this report, an automatic amplitude picker in ProMAX was used to pick the peak maxima along the event while the event was flattened.

RESULTS

In Figure 3 we show a close-up of the NMO-corrected reflection event at 1315ms. For purposes of measuring reflection amplitude, it is important to measure the reflection from the top of the reflection in the model on the *first significant peak* of the event, since all subsequent parts of the waveform may be contaminated by the ghost events attributable to the water layer. The experiment was designed so that the ghost arrivals would be well separated from the initial reflection event itself, since ghosts are not included in the AVAZ theory being tested. The peak at 1315ms was identified by Mahmoudian as the reflection of interest, and Figure 3 shows the event itself in the lower part of the figure, with all of the interference from direct arrivals and the shallower Plexiglas reflection. The upper plot is the actual event amplitude as picked along the maximum of the peak of the event. The large variance of the plotted amplitude values immediately illustrates the problem encountered by anyone hoping to use the amplitudes for verifying AVAZ theory.

Figure 4 shows the phenolic layer reflection in variable density display, on an expanded time scale to illustrate the varying slopes of the interfering event wavefronts. Each of the following figures shows the phenolic event after RT filters were applied to the trace gather to remove successively identified interference events. After each filter application, which is a *subtraction* of estimated noise, the event amplitudes were picked along the peak maximum of the event and plotted in the upper portion of the figure.

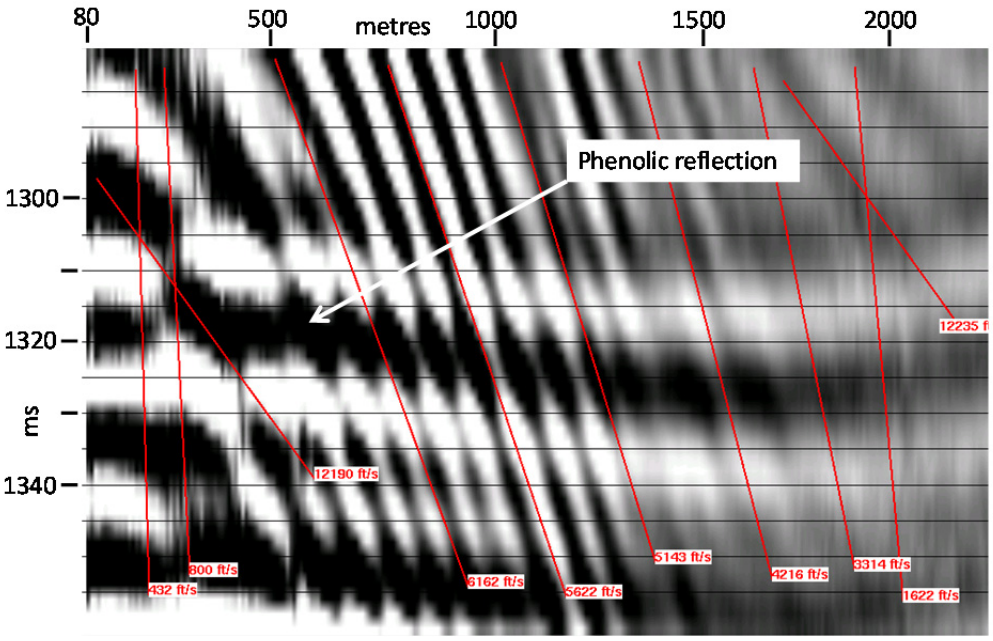

FIG. 4. Zoom of the phenolic event and interference. Several event 'velocities' have been indicated.

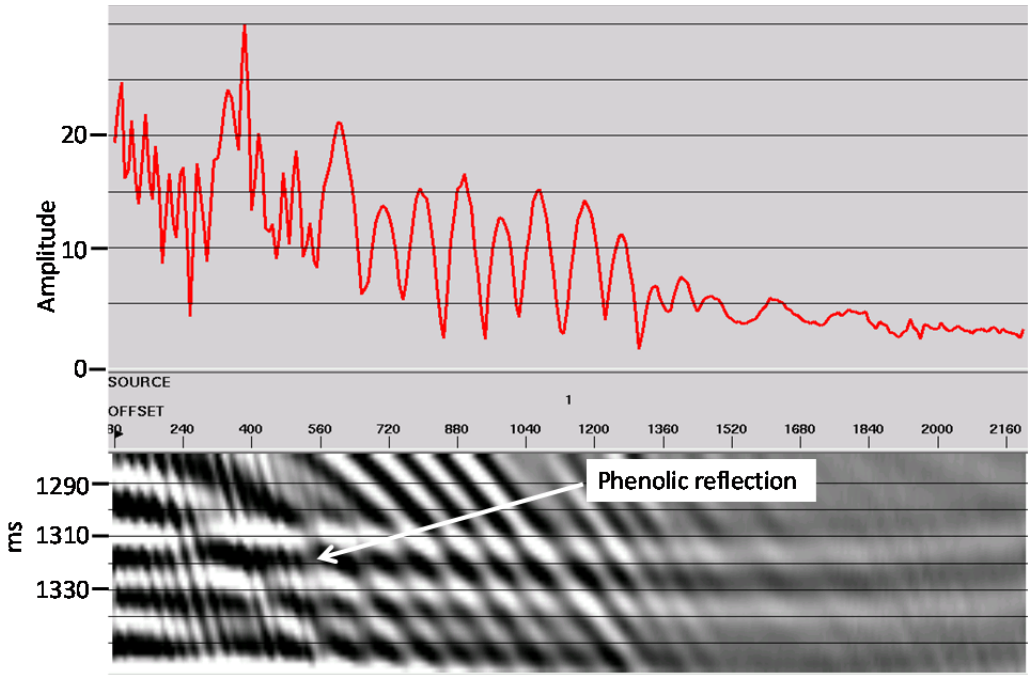

FIG. 5. Direct water arrival event removed by RT fan filter—compare long offsets in Figure 3.

Figure 5 shows the result of applying an RT fan filter to the raw shot gather before application of NMO correction (although NMO was applied in order to conveniently display and pick the event amplitudes). As can be seen by comparison with Figure 4, the interference at long offsets has been largely removed, as has some of the interference at shorter offsets (more apparent in the amplitude plot than on the event itself). When we applied an RT dip filter with the velocity of the direct arrival (1480m/s—water velocity) to the gather, still before NMO correction, the result is shown in Figure 6. In this step, much of the interference from the repeated direct arrivals at shorter offsets has disappeared, both on the event itself, and on the amplitude plot.

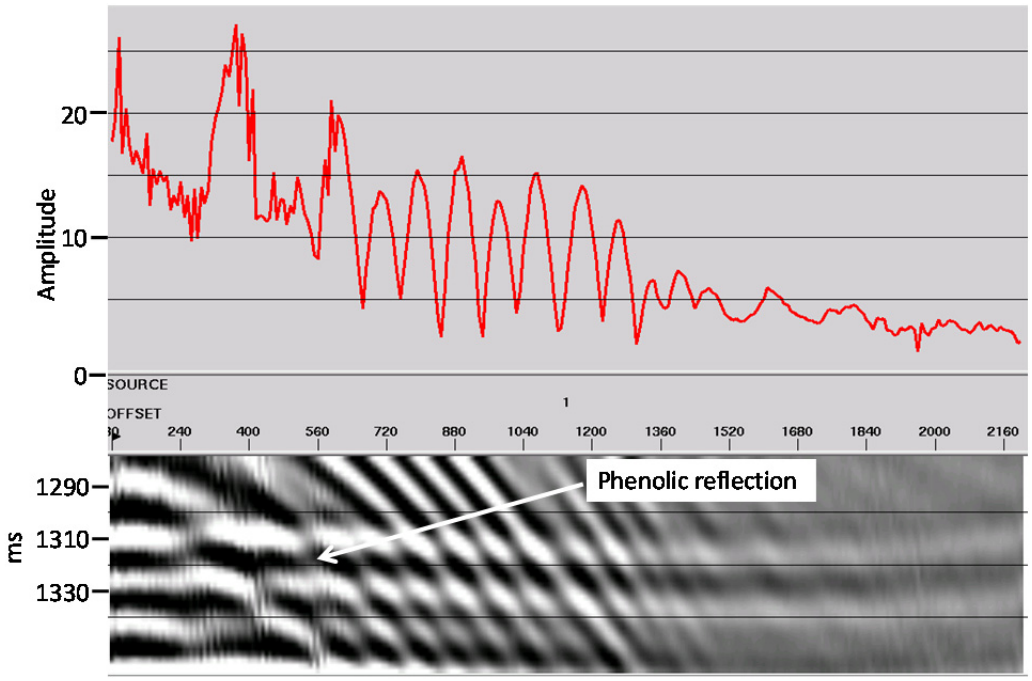

FIG. 6. Direct water arrival, ghosts, and repeats removed by RT fan filter and RT dip filter.

We then applied NMO to the event, and applied a series of RT dip filters to attenuate the visible interfering events. In this procedure, we analyzed the apparent velocity of each interfering event or group of events and applied a dip filter of that velocity to estimate and subtract the event. Figure 7 shows the result of the first step in this process—a dip filter with a velocity of approximately half that of the water-borne direct arrival (800m/s). By comparing with Figure 6, we see that this step removed the very short-wavelength, steep events at the shorter offsets (probably aliased from the repeated direct arrivals). In Figures 8, 9, 10, 11, and 12, we show the results of successively applying RT dip filters of increasingly higher apparent velocity (1500m/s, 3000m/s, 4000m/s, 5000m/s, 6000m/s, 8000m/s, 12000m/s, 14000m/s, and 16000m/s). In each case, the slope of the dip filter approaches that of the target reflection (basically flat—infinite velocity) more and more closely at the near offsets. At the highest velocity, the pass band of the interfering event may infringe on the reflection pass band, as well. Hence, as we view the figures in succession, we observe the successive removal of interference and the subsequent reduction of the variance of the amplitude measurements, while the amplitude *trend* (as a function of offset) that we seek for AVAZ measurements remains intact.

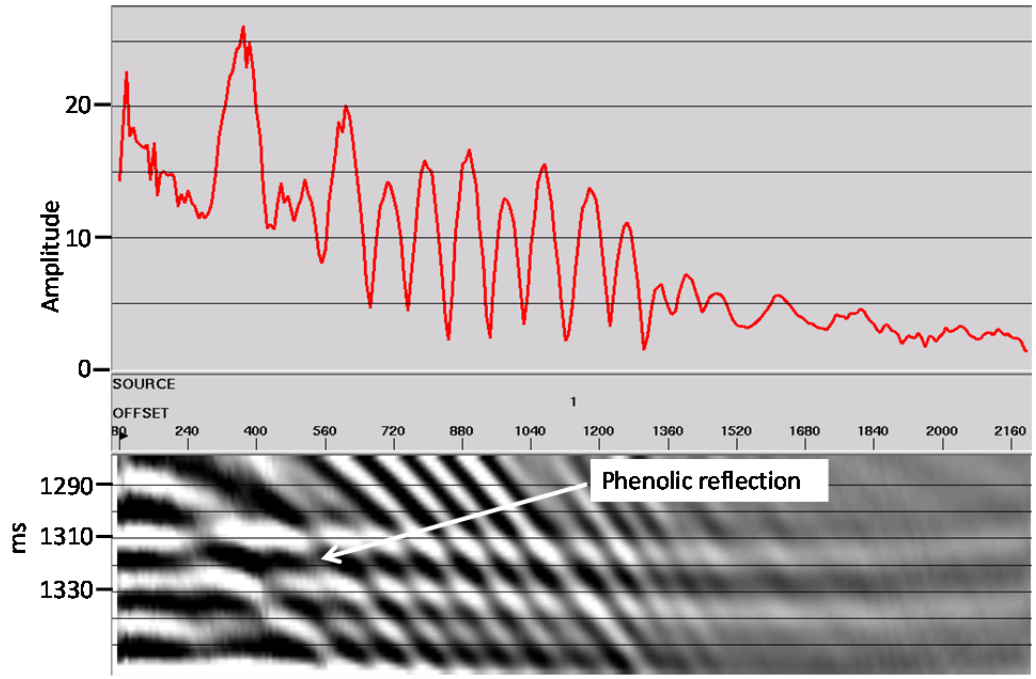

FIG. 7. Near-offset interference reduced by +/- 800m/s RT dip filters after NMO correction.

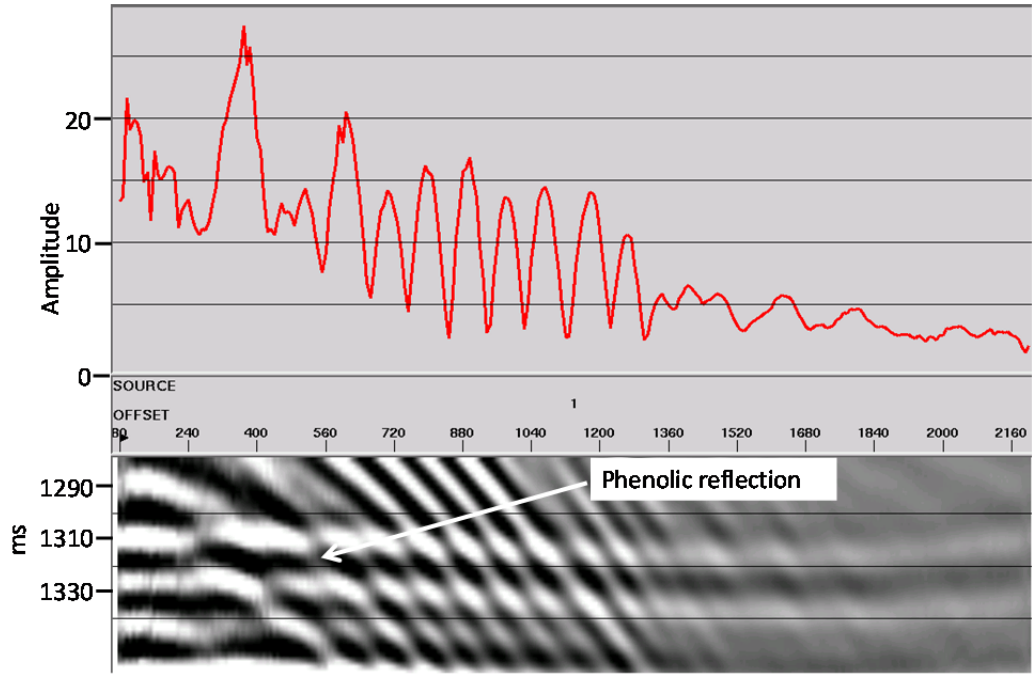

FIG. 8. Far-offset interference reduced by RT dip filters at +/-1500m/s and +/-3000m/s.

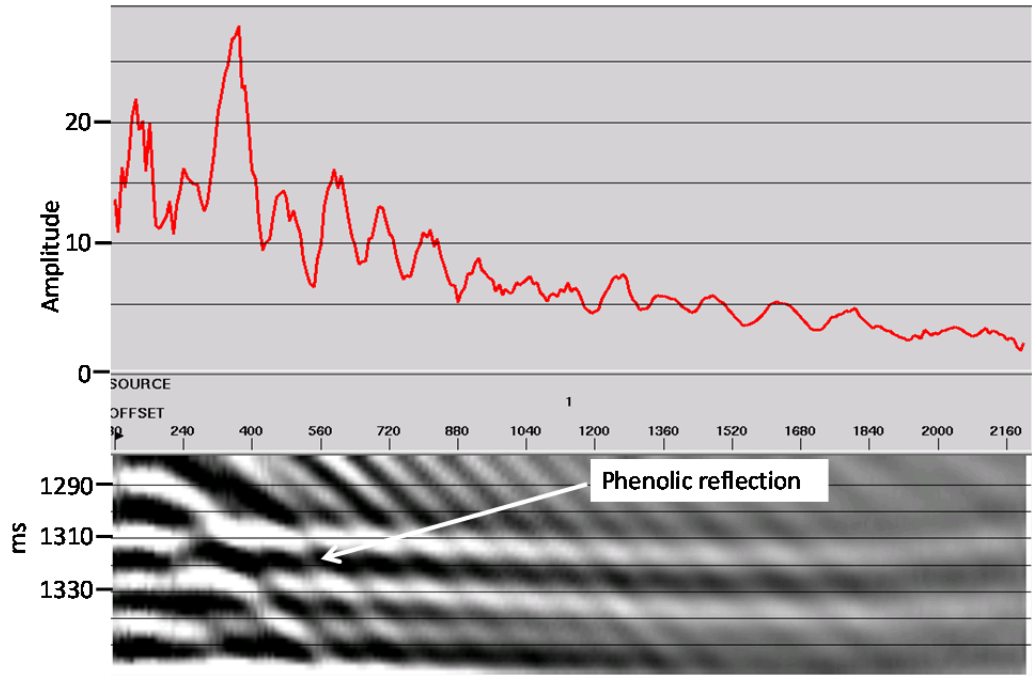

FIG. 9. Intermediate-offset interference reduced by RT dip filters at +/-4000m/s and +/-5000m/s.

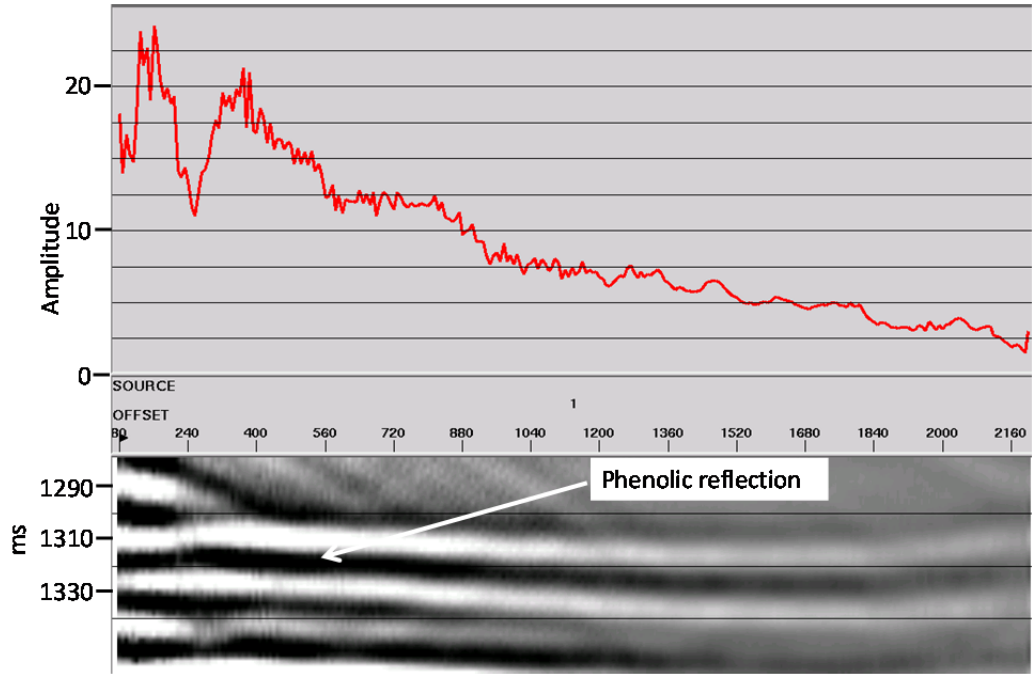

FIG. 10. More interference removed by RT dip filters at +/-6000m/s and +/-8000m/s.

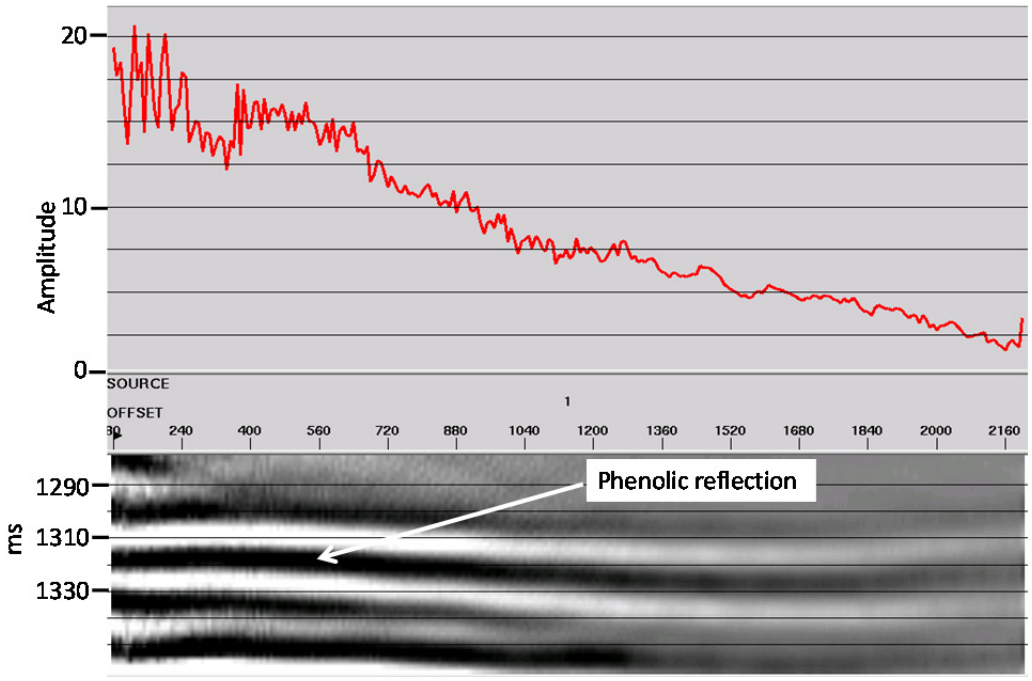

FIG. 11. Near-offset interference reduced by RT dip filters at +/- 12000m/s and +/-14000m/s.

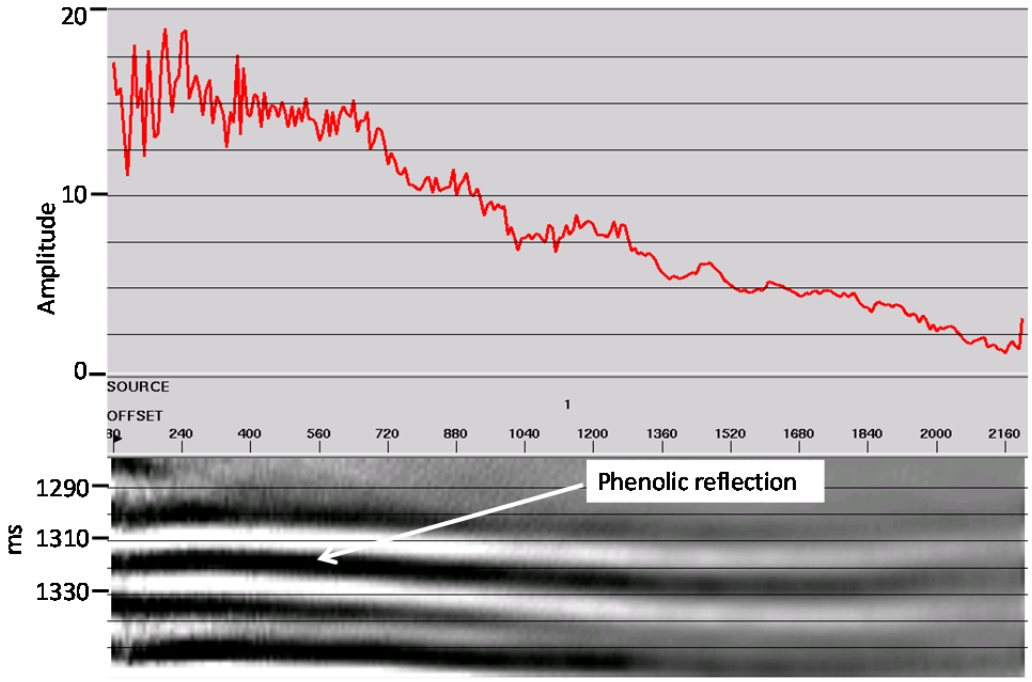

FIG. 12. Final noise reduction using RT dip filters at +/- 16000m/s.

However, when applying the RT filter of the highest velocity, we began to observe that the reflection amplitude at the very nearest offsets, where the target reflection is very nearly parallel to the shallower reflection, is attenuated as well. While it is possible, by much careful trial and error, to design a set of RT filters that has minimal effect at short offsets while removing most of the reflection amplitude variance due to interference over

most of the offset range, we display here one set of results for five different azimuths, where the interference has been dramatically reduced for *most* of the offset range, except for the *nearest offsets*. Figure 13 shows the result for zero degrees azimuth, while Figures 14, 15, 16, and 17 show the results for azimuths 14deg, 27deg, 37deg, and 45deg, respectively.

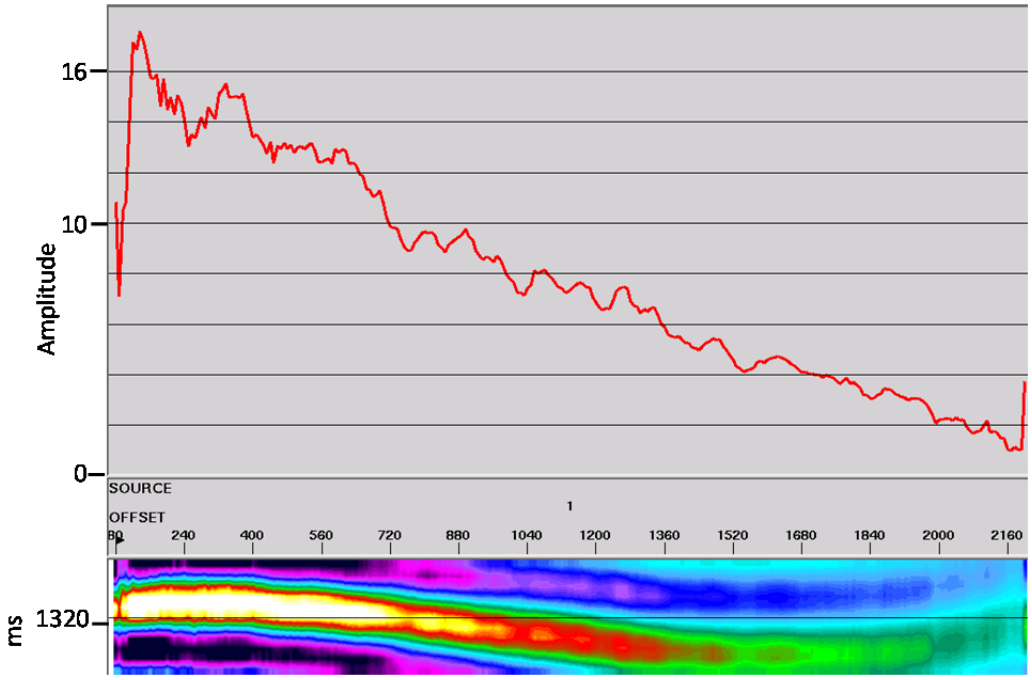

FIG. 13. Final AVO profile for azimuth 0 degrees. Windowed event is at the bottom.

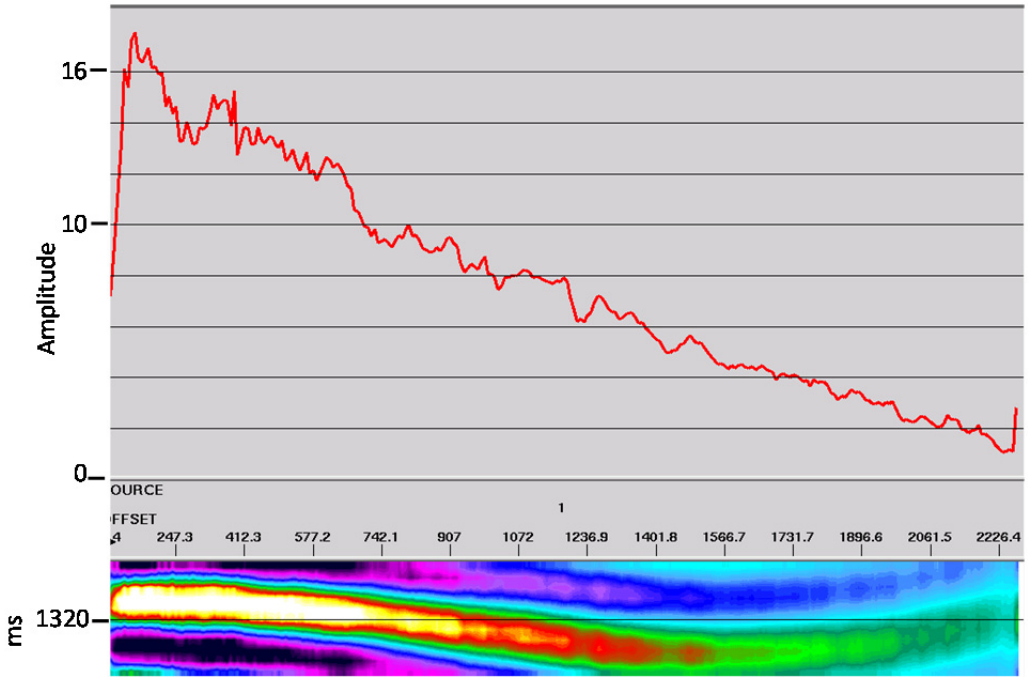

FIG. 14. Final AVO profile for azimuth 14 degrees. Windowed event is at the bottom.

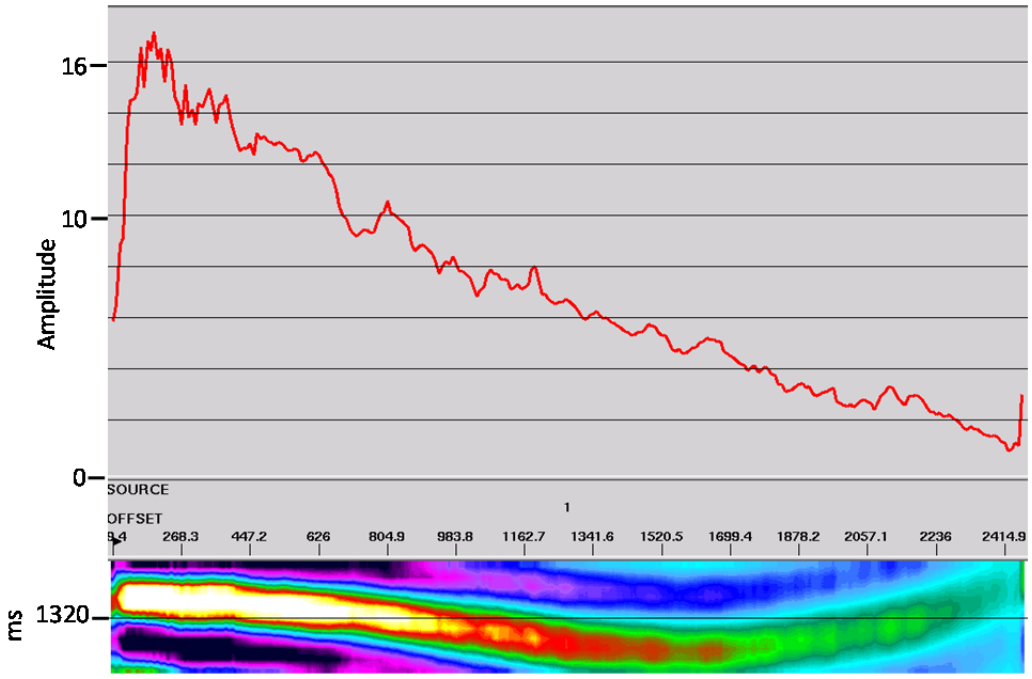

FIG. 15. Final AVO profile for azimuth 27 degrees. Windowed event is at the bottom.

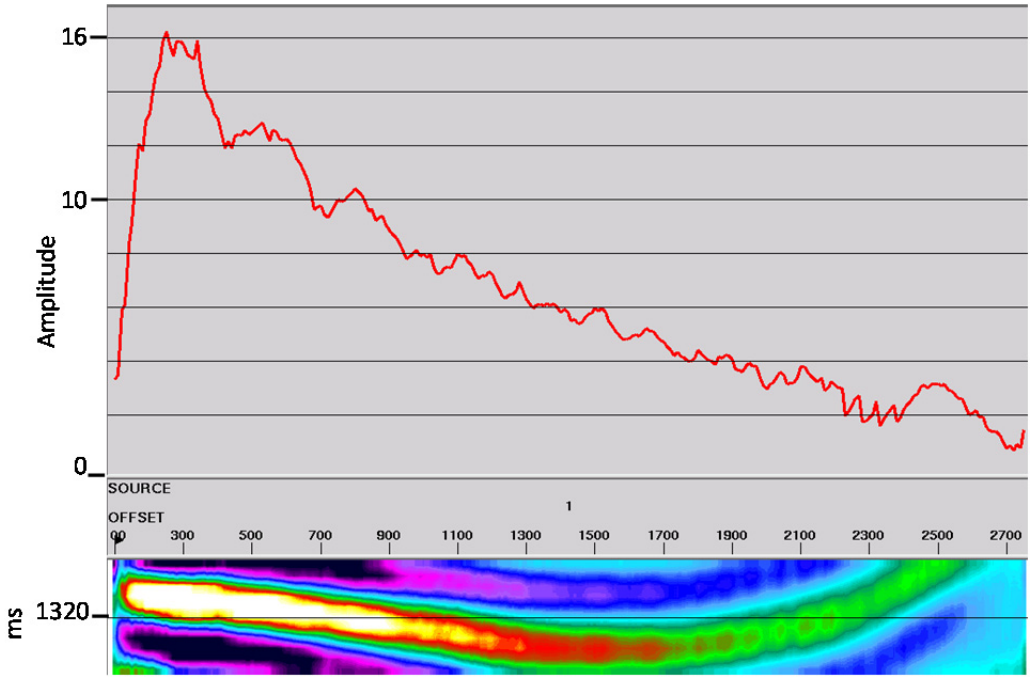

FIG. 16. Final AVO profile for azimuth 37 degrees. Windowed event is at the bottom.

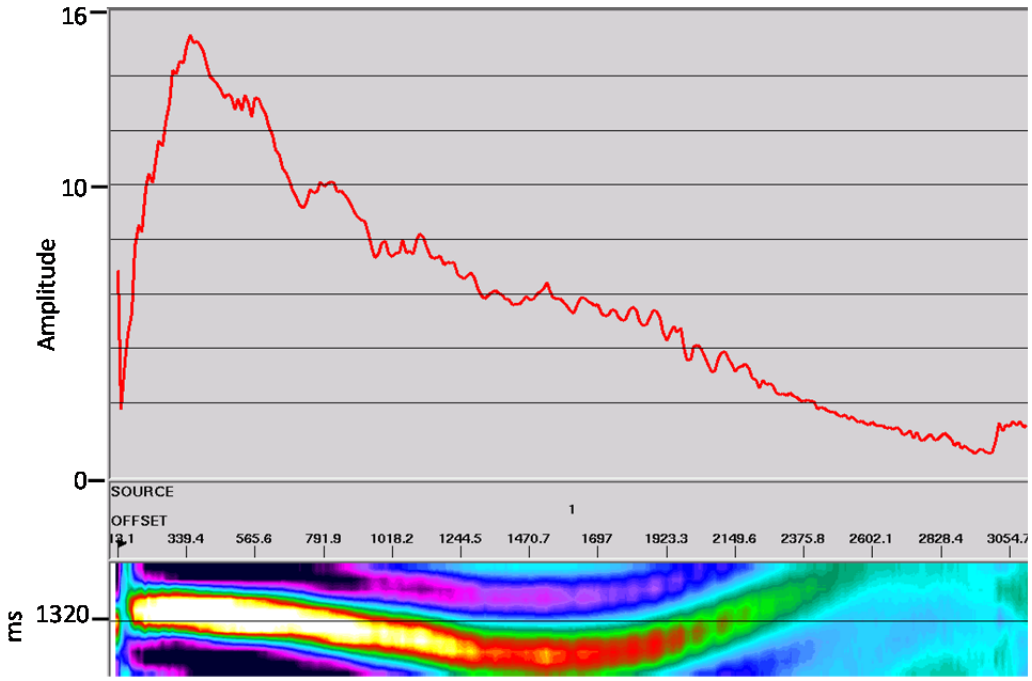

FIG. 17. Final AVO profile for azimuth 45 degrees. Windowed event is at the bottom.

DISCUSSION

The use of RT filtering has been described thoroughly in other material, usually in the context of de-noising entire source gathers early in a data processing sequence. Here, we have focussed on a very specific application, where our main interest is removing as much coherent interference as possible from a single reflection event so that its amplitudes can be accurately estimated for AVAZ studies. We determined that it is possible, using a very interactive approach, to design a set of filters that significantly removes interference with little effect on underlying reflection amplitudes. At each stage in the process, it is important to ensure that the low-pass filter parameters are such that the reflection passband is excluded as much as possible. At some point, however, there is an RT filter velocity (slope) which is so close to that of the target reflection at near offsets that no matter how the passband of the filter is restricted, it will overlap that of the reflection and affect its amplitudes. This limiting velocity is most easily determined via trial and error.

The filter parameters for each azimuth in an AVAZ survey need to be determined individually, since the apparent velocities of a model may change with azimuth (due to slight levelling errors in the model). This affects the apparent velocities of the interference pattern, as well as the required NMO for the reflection event.

ACKNOWLEDGEMENTS

We are grateful to Joe Wong for data acquisition and to Gary Margrave for leading the AVAZ project. We also acknowledge CREWES sponsors and NSERC for financial support.

REFERENCES

Henley, D.C. 2003, Coherent noise attenuation in the radial trace domain, Geophysics, **68**, No. 4, pp1408-1416.

Henley, D.C., 2011, Now you see it, now you don't: radial trace filtering tutorial, CREWES research report—Volume 23(2011).

Henley, D.C., and Wong, J., 2013, Through the looking glass: using X-T plane distortions for wavefield separation, CREWES research report—Volume 25(2013).

Mahmoudian, F., Margrave, G.F., Daley, P.F., and Wong, J., 2012a, Anisotropy estimation for a simulated fractured medium using traveltime inversion: a physical modeling study: SEG 82nd Annual Convention, Expanded abstracts.

Mahmoudian, F., Wong, J., and Margrave, G.F., 2012b, Azimuthal AVO over a simulated fractured medium: A physical modeling experiment, SEG 82nd Annual Convention, Expanded abstracts.

Mahmoudian, F., 2013a, Physical Modeling and Analysis of Seismic Data from a Simulated Fractured Medium, PhD. Thesis, University of Calgary.

Mahmoudian, F., Margrave, G.F., Wong, J., and Henley, D.C., 2013b, Fracture orientation and intensity from AVAZ inversion: a physical modeling study, SEG 83rd Annual Convention, Expanded abstracts.

Mahmoudian, F., Margrave, G.F., Daley, P.F., Wong, J., and Henley, D.C., 2013c, Estimation of anisotropic elastic stiffness coefficients of an orthorhombic physical model using group velocity analysis, accepted for publication in Geophysics.

Wong, J., and Mahmoudian, F., 2011, Physical modeling II: directivity patterns of disc transducers, CREWES Research Report — Volume 23 (2011)